technologies

Article

Statistical Evaluation of Robot Trajectories in Automated Dimensional Measurements

Aleš Zore * and Marko Munih

Faculty of Electrical Engineering, University of Ljubljana, 1000 Ljubljana, Slovenia; marko.munih@fe.uni-lj.si
* Correspondence: ales.zore@fe.uni-lj.si

Abstract

The influence of a robot's manipulation can be observed in a robotic measurement system. Different robot end-effector trajectories yield different robot end-effector accuracy and repeatability errors. Trajectory parameters, robot motion type, velocity, and length of motion were identified as influential sources. A robot arm was used to insert measuring objects into the measurement device for dimensional measurements. In the first part, the measurement datasets for linear and joint robot motions were compared for three different velocities and four motion lengths. The influence of the number of active joints in the robot's motion was compared for two velocities and four magnitudes of joint rotation. Dimensional measurement variability was analysed using measurement system analysis (MSA), and the statistical influence of trajectory parameters was further addressed by analysis of variance (ANOVA). All identified trajectory parameters have a statistically significant impact on measurement variability, reflecting the robot end-effector's accuracy and repeatability errors. Linear motion provides higher measurement variability up to 20%, a velocity increase that is typically up to 25–35% and motion length that is typically up to 15–35%.

Keywords: robot; dimensional measurements; trajectory; velocity; distance; number of active joints

1. Introduction

The increasing emphasis on higher product quality in the process industry requires the continuous development of the manufacturing process. Heavy demands on dimensional tolerances require the ever-improving development of the manufacturing process or enhancements in quality control.

In the past, various approaches have ensured sufficient product quality and manufacturing process control. For example, in the automotive industry, statistical process control (SPC) [1–3] is an established method of quality and process control. Several SPC techniques (histograms, control charts, and scatter diagrams) can be used to evaluate the capability of the manufacturing process.

Two-stage quality and process control are primarily used in industry. The first stage consists of frequent manual measurements performed by operators. The second stage consists of measuring selected samples at a lower frequency using a reference measuring device. The coordinate measuring machine (CMM) has a leading role in manufacturing metrology. In addition to its good properties, such as high accuracy, precision, and resolution, the CMM also has significant disadvantages, including time complexity and temperature dependence.

Academic Editor: Manoj Gupta

Received: 6 March 2026
Revised: 20 April 2026
Accepted: 23 April 2026
Published: 26 April 2026

 https://doi.org/10.3390/technologies14050261

Due to time-consuming CMM operations, the product's measurement data are not evaluated in real time, as an unavoidable delay is present. In addition, the CMM's measurement uncertainty is also affected by the selected measurement procedure (fitting algorithms [4–6], sampling strategy [7,8], measurement method [9–12]), the measuring equipment [6,10,13–16] and the influence of an operator [10,11].

Using the CMM in the comparative mode eliminates the kinematic part of the measurement uncertainty and reduces the part associated with environmental impacts [15,17,18]. Further, automation and robotisation of dimensional measurements reduce the time required for the measurement process, increase the reliability of the measurement system and reduce or eliminate the influence of the human operator [19–27]. Consequently, the number of inspected samples can be increased, thereby reducing the delay in manufacturing control.

The primary role of quality assurance is elementary, i.e., always measure in the same way. Industrial robots have good properties in terms of accuracy and repeatability, and thus meet the requirements for performing quality-assurance operations consistently.

The authors of studies on a robot's accuracy and repeatability most often highlighted the effects of the robot's motion velocities [28–32], the payloads on the tool centre-point (TCP) [28,31–34], the length of the robot's motion [29,32,33], the locations of the robot's end-effector in the workspace [35,36], mechanical errors [37], and, last but not least, the influences of the kinematic models [38–42].

The calculated values of the robot's accuracy and repeatability are based on measurements of the robot's end-effector pose [28–33,35,36,43,44] or based on calculations of kinematic and error models [37–39,41].

However, there is no emphasis on the influence of the robot and its manipulation on the measurement process or the measurement uncertainty of the measurement system. Aminabadi et al. [27] used an industrial robot arm to deliver objects from an injection moulding device into an optical measurement system. Robot manipulation produced positional displacement and, consequently, increased measurement error. Further, Zore et al. [45] showed that, in dimensional contact measurements with the robot manipulating the measuring objects, different degrees of robotic manipulation have distinct effects on the variability of the dimensional measurements. Manipulation with robots within the measurement system, in principle, influences the repeatability and overall capability of the whole measurement system.

An important factor in measurement uncertainty is the object's positioning in the measuring device. When serving objects into the measuring device, robots introduce less positional error compared to a human operator. Lemes et al. [22,46] used a five-axis robot for a robot serving CMM. The robot held the object during the measuring process. Thus, the measurement uncertainty also included the robot's vibrations. Zore et al. [45] and Aminabadi et al. [27] inserted the object into the fixture of the measuring device and then moved the robot outside the measuring device's working area. The measurement uncertainty of the dimensional measurements in this way did not account for the robot's vibrations.

In the previous study, the focus was on whether the variability of dimensional measurements, which is directly related to measurement uncertainty, varies across different levels of robot manipulation complexity. The current focus is narrower and aims to investigate the influence of robot trajectory parameters on the dimensional measurements' variability. The goal of this research is to identify how the robot affects the measurements and not to achieve an improvement by incorporating the robot. Based on research into an industrial robot's accuracy and repeatability, the robot's motion velocity, the length of the robot's motion, the motion type, and the number of active joints were identified as four influential parameters of the robot's end-effector trajectory.

Due to robot manipulation, the measured object may exhibit positional or orientation deviations during insertion into the measurement device. A slight pose deviation yields different measured dimensions (in µm scale), thereby increasing dimensional measurement variability.

Unlike the presented methods for robot accuracy and repeatability, our research is not based on measurements of the robot's end-effector position. Instead, changes in dimensional measurement variability indicate the robot's accuracy and repeatability errors. The greater the variability of the measurements, the greater the influence of the robot's trajectory on the accuracy or repeatability of the robot end-effector.

The main findings from the presented research on the influence of motion type, velocity, and motion length are readily applicable to precise pick-and-place applications to minimise end-effector pose error. Further, the optimal positioning of the measuring device and the pallet with the objects relative to the robotic arm can be optimised in a fully automated/robotised measurement process.

A robot arm was used to insert measuring objects into the measuring device. To investigate the influence of individual trajectory parameters, such as motion type, motion velocity, and motion length, experiments produced 43 different robot motion scenarios. After all sets of robot motion and dimensional measurements, statistical evaluations using MSA (measurement system analysis) [3,47] and ANOVA (analysis of variance) were performed. Statistical analysis shows that linear end-effector motion produces greater variability in dimensional measurements than joint motion, higher motion velocities further increase measurement variability, and motion length has a perceptible impact.

2. Measurement System and Objects

An advanced robot cell (Figure 1) was used to investigate the effects of the robot's trajectory parameters on contact dimensional measurements. A more detailed presentation of the robot cell is presented in [45]. A Universal Robots UR5e collaborative robot was used to manipulate the objects and a Renishaw Equator comparator principle-based measurement system was used to perform the contact's dimensional measurements.

Comparator principle-based measurements eliminate the kinematic component of measurement uncertainty and reduce the component associated with environmental impacts [15,17,18]. Systematic effects associated with the measurement system apply to both the test and master artefacts, and a substantial proportion of the systematic effect cancels out between the two sets of measurements.

As presented in the previous study [45], two types of mass products were selected, i.e., a magnet and a PKR. Both objects represent products in automotive manufacturing. The object magnet has a hollow, cylinder-like shape for rotors, and the object PKR is a commutator for a starter motor. This investigation covers the most critical dimensional characteristics included in the SPC measurements for each object. In the case of the magnet object, two dimensional characteristics, magnet diameter (characteristic 20) and magnet height (characteristic 30) were studied (Figure 2a). In the case of the PKR object, four dimensional characteristics, one diameter—groove diameter (characteristic 130)—and three heights—base height, height to wrench and groove depth (characteristics 10, 100 and 140, respectively)—were targeted (Figure 2b). Therefore, six dimensional characteristics are the subjects of this study, including two diameters and four length measurements.

To fix the measuring objects, magnet and PKR, special fixtures were designed (Figure 2c). The fixtures are designed to allow robot interventions and satisfactory fixations while also enabling access to measuring features (characteristics) with measuring probes of the Equator. The fixture mandrel fits the outer diameter to the inner diameter of the measuring object, and a spring ball inside the mandrel provides better stability for the

https://doi.org/10.3390/technologies14050261

measuring object. Due to the different internal diameters, two different fixtures were used for the object magnet and PKR separately.

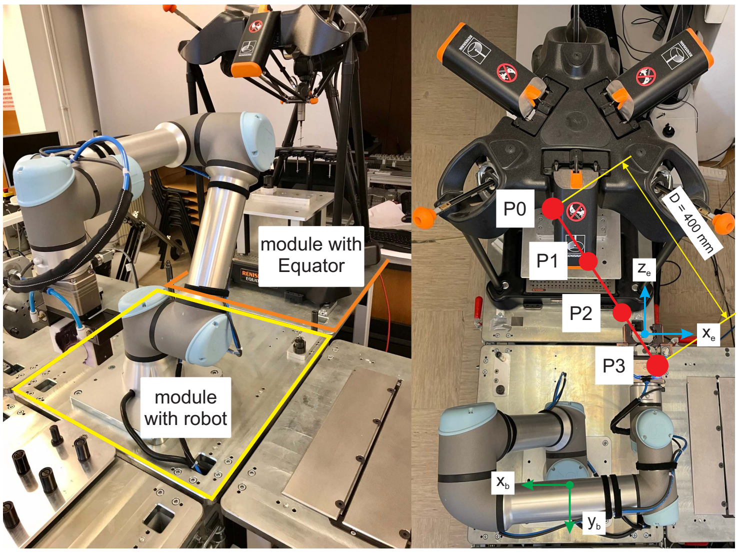

Figure 1. The Ur5e robot and the Equator measuring device in the adaptive robot cell (**left**). A top-view illustration of a virtual line with the points P0, P1, P2 and P3 (**right**). The robot's base frame is coloured green and the robot's end-effector frame is coloured blue.

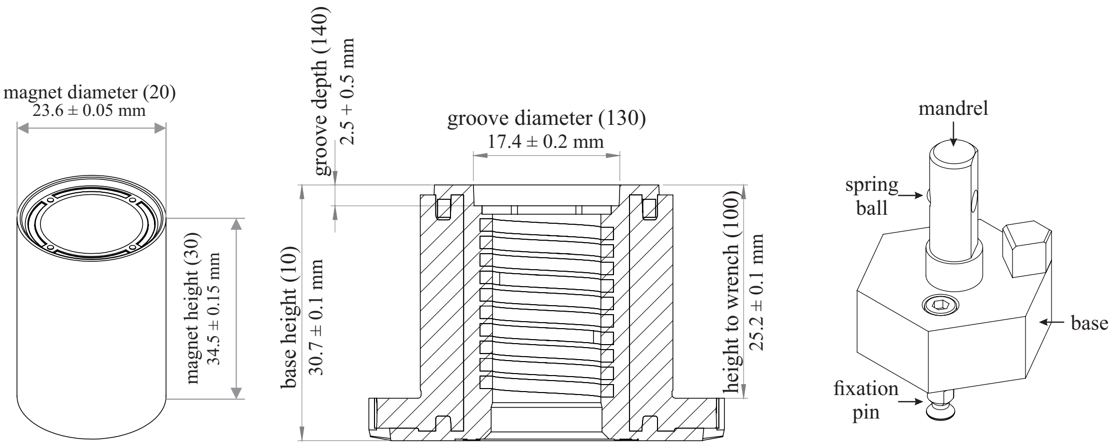

(**a**) Magnet object (**b**) PKR object (**c**) Fixture

Figure 2. (**a**) Magnet object with measured characteristics, (**b**) PKR object with measured characteristics, and (**c**) fixture design.

3. Robot Trajectory Experiments

The hypothesis is that varying the robot trajectory parameters while manipulating the objects results in a pose variation of the inserted object. As a consequence, the variability of the dimensional measurements changes. Using the comparator principle-based measurement system Renishaw Equator, robot accuracy and repeatability errors will be indirectly estimated by observing the variability in dimensional measurements resulting from the choice of robot trajectory parameters.

The influential sources of robot trajectory, robot motion type, motion velocity, and motion length were identified. The study is divided into two main parts. The first part emphasised the variability of the measurements depending on the motion type of the robot end-effector, namely linear or joint motion (Section 3.1). The second part focuses on the variability of the measurements resulting from the number of active joints that generate the robot's motion (Section 3.2).

3.1. Robot Interpolation Motion Type Comparison

In the first part, the robot end-effector moves with linear or joint motion, and it has different effects on the variability of the contact's dimensional measurements. In other words, different interpolation methods of the intermediate robot poses have different effects on the variability of the measurement results. In addition to the influence of the robot's end-effector trajectory, the influence of the robot's movement velocity and the length of the movement were investigated.

For this purpose, a virtual line with one endpoint at P0 = (45.5, −675.0, 393.3) mm (50 mm above the fixture in the Equator working space) and another at P3 = (−237.3, −392.2, 393.3) mm, 40 cm away from P0, was created. The experimental setup used in our study is shown in Figure 1, together with a representation of the virtual line with points P0, P1, P2 and P3. The virtual line lies parallel to the XY plane and is divided into three equal parts, with two intermediate points, P1 = (−48.8, −580.7, 393.3) mm and P2 = (−143.1, −486.4, 393.3) mm. The robot is capable of performing motions from points P1, P2 and P3 to point P0, either by linear or joint motion, without colliding with the Equator frame or crossing the robot's singularities. Points P0, P1, P2 and P3 serve as the start and stop poses of the robot's end-effector in individual scenarios.

The reference scenario, with the least amount of robot manipulation, is the scenario with P0 selected as a starting point. The robot holds the object in the gripper (with 30 N), then vertically inserts it into the fixture and releases it. Object placement is always followed by the robot's retraction from the Equator's working area, which triggers the dimensional measurements of the object. The Equator completes the dimensional contact measurements, after which the robot approaches the object in the fixture, grasps it, and performs a backward movement to point P0, completing the execution cycle.

The remaining scenarios are very similar, with the robot adding more manipulation. By selecting different starting/end poses, the robot's motion length differs. The robot pre-holds the measuring object in the selected pose (P1, P2 or P3) and moves to pose P0. The identical cycle, as in the reference scenario (object placement, dimensional measurements, and object removal), is followed. Finally, the robot completes the cycle again in the selected starting position (P1, P2, or P3).

Robot end-effector orientation in P0, P1, P2 and P3 is identical and is defined using Euler angles roll, pitch and yaw $RPY = (90°, 0°, 180°)$. In this case, linear motion nominally does not change the robot's end-effector orientation, and the TCP follows the virtual line. Of course, this is not valid for robot joint motion.

A single measurement set consists of 25 repetitions of object manipulation from the starting pose (P0, P1, P2, or P3), object insertion, dimensional measurements and object removal. A measurement set is repeated for the linear and joint trajectory movements of the robot. Furthermore, the velocity of the robot's movements was varied among start poses P1, P2, and P3 to pose P0 within Equator's working area (above fixture), respectively. In the case of linear motion, we performed measurements at three different linear velocities of the end-effector, i.e., 0.3 m/s, 1.5 m/s and 2.5 m/s. In the case of joint movements, the joint velocities were 0.5 rad/s, 1.5 rad/s and 3.0 rad/s. Vertical robot trajectories for object placement and removal were constant for all trajectory variations between poses P1/P2/P3 and P0. Measurements were repeated three times for each trajectory parameter selection (motion type, motion length and motion velocity) to satisfy statistical criteria.

3.2. Number of Active Joints

The second part focuses on measurement variability arising from the number of active joints that generate the robot's motion. For this, four new robot-manipulation scenarios were designed, from one active joint to four active joints (Table 1). Only the fifth joint (Wrist 2) is active in the first scenario. The second and third joints (Shoulder and Elbow) are active in the second scenario. In the third scenario, the second, third and fourth joints (Shoulder, Elbow and Wrist 1) are active, and in the last scenario, the second, third, fourth, and fifth joints are active (Shoulder, Elbow, Wrist 1 and Wrist 2). The joint nomenclature is conventional for this type of robot.

Table 1. Representation of the active joints in the second part and the joint angle step $\Delta\varphi$. Naming of robot joints: B—Base, S—Shoulder, E—Elbow, W1—Wrist 1, W2—Wrist 2 and W3—Wrist 3.

Scenario	**B**	**S**	**E**	**W1**	**W2**	**W3**	$\boldsymbol{\Delta\varphi}$
W2					✓		30°
SE		✓	✓				20°
SEW1		✓	✓	✓			20°
SEW1W2		✓	✓	✓	✓		20°

A representation of the robot UR5e joints and axes is shown in Figure 3. The robot joints are, from the bottom up, labelled as follows: **B**ase, **S**houlder, **E**lbow, **W**rist **1**, **W**rist **2** and **W**rist **3**.

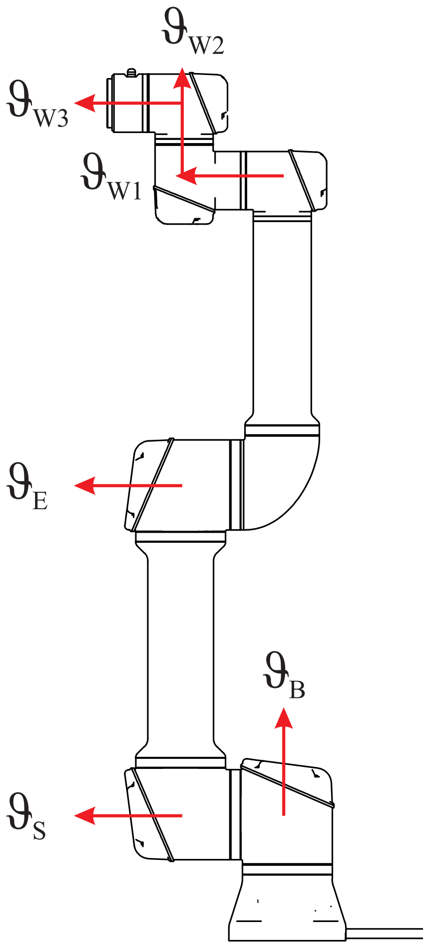

Figure 3. A representation of robot UR5e joint axes. Names of robot joints: B—Base, S—Shoulder, E—Elbow, W1—Wrist 1, W2—Wrist 2 and W3—Wrist 3.

Combinations of different velocities were also implemented while observing dimensional measurement variability. The measurement scenarios were repeated for two joint velocities, i.e., 0.5 rad/s and 3.0 rad/s. Note that the linear movement of the end-effector could not occur as only some of the robot's joints were activated. Whether the magnitude of the joint's rotation affected the variability of the object's measurements was also monitored. To this end, measurements were performed for three joint angle rotations at each velocity. In scenario W2, the joint angles were $\varphi = (0^\circ, 30^\circ, 60^\circ, 90^\circ)$, and in the remaining cases, the joint angles were $\varphi = (0^\circ, 20^\circ, 40^\circ, 60^\circ)$. In the scenario W2, the robot configuration and space in the Equator working area enabled larger joint rotations. With larger joint rotation, the influence could be more significant and was easier to see. Please note that joint angles $\varphi = 0^\circ$ coincide with pose P0 in the first part of the measurement scenarios.

A selected scenario with the desired joint rotations was performed prior to vertical object insertion and dimensional measurements. The insertion, measurement operation and object removal were identical to those in the first part.

As was the case in the first part, each combination of scenario and trajectory parameters was repeated three times.

3.3. Statistical Analysis and Evaluation

The dimensional measurement procedure consists of 25 repetitions of moving the robot with the object from the initial robot pose, inserting the object into the fixture, taking dimensional measurements, removing the object from the fixture and moving the robot back to the initial robot pose.

Each of the scenarios in the first (Section 3.1) and second part (Section 3.2) consists of three measurement sets (repetitions) for the appropriate statistical evaluation.

The first part of the measurements includes the influence of the robot's trajectory for two motion types (=2) at three different velocities (=3) and three distances (P1, P2 and P3) (=3). Together with the measurements at point P0, this produces $2 \cdot 3 \cdot 3 + 1 = 19$ different robot trajectories/measurement scenarios. Considering the data for six geometric characteristics of two objects (=6), three repetitions of the measurement sets (=3) and 25 measurements within one set, we have $19 \cdot 6 \cdot 3 \cdot 25 = 8550$ dimensional measurements in the first part. In the second part, measurements of four manipulation scenarios (=4) at two velocities (=2) and three magnitudes of the joint rotations (=3) are added, i.e., $4 \cdot 2 \cdot 3 = 24$ new measurement scenarios and consequently $24 \cdot 6 \cdot 3 \cdot 25$ = 10800 dimensional measurements (6, 3 and 25 have the same explanation as above). Together, the study consists of 8550 + 10800 = 19350 dimensional measurements.

The measurement approach is based on the Measurement System Analysis (MSA) procedure 1—Systematic Measurement Error and Repeatability [3]. For the measurements, reference objects were used, one magnet and one PKR, which were previously measured on a coordinate measurement machine (CMM). The results of the MSA analysis are numerous statistical parameters, among which the most important are the process/measurement capability C_g and the standard deviation σ. Their mutual correlation is given in Equation (1), where T is the defined tolerance range for the geometric characteristic.

$$C_g = \frac{0.2\,T}{6\sigma} \tag{1}$$

The MSA usually focuses on the value of six times the standard deviation (6σ), as it is calculated directly from the given measurements and is independent of the tolerance range of the geometric characteristic.

In a previous study [45], the normal distribution of the dimensional contact measurements was confirmed using the Anderson–Darling [48] normality test with 95% confidence level, so the selected statistical method (MSA) can be used for statistical evaluation. Corresponding p-values, which should be higher than $p_{min} = 0.005$, are 0.91 and 0.75 for dimensional characteristics of the magnet object, and 0.74, 0.23, 0.59, and 0.97 for the PKR object.

The homogeneity of the measurement data groups was tested using the Brown–Forsythe homogeneity test [49]. In all cases, the resulting p-value was $p \gg 0.05$, indicating that the data sample groups' variances did not differ significantly. The lowest calculated p-value was $p = 0.4011$.

The normal distribution and homogeneity of the measurement results further enabled the use of the analysis of variance (ANOVA) method to statistically determine the significance of the individual parameters of the robot's end-effector trajectory for the 6σ value. The change in variability (6σ) with a single parameter change would determine the influence of the trajectory parameter on dimensional measurements.

4. Results

Thissection contains the results of the effects of the individual robot-trajectory parameters on the dimensional measurements. In the first part, a comparison of the influences of the robot's linear and joint motions on the dimensional measurements is presented. In the second part, the impact of the robot's trajectory when using different numbers of active joints to perform the motion is evaluated. The statistical significance (determined via the ANOVA method) of the trajectory parameters' motion type, motion velocity, motion length, and number of active joints, as they relate to dimensional measurements, is shown at the end of the Results Section.

For each repetition of the $19 \cdot 6 \cdot 3$ scenarios for the first part and $24 \cdot 6 \cdot 3$ scenarios for the second part, an MSA type-1 analysis was performed for each of the six dimensional characteristics (25 values). The selected statistical characteristic obtained from the MSA study, among others, is 6σ (six times the standard deviation).

4.1. Linear vs. Joint Movements

Graphs presenting the values of 6σ depending on the motion type (linear or joint motion), motion velocity, and length of the motion are shown in Figures 4 and 5.

The measurement data calculated using the MSA type-1 analysis for the dimensional characteristic magnet diameter (20) and magnet height (30) of the object magnet are shown in Figure 4a,b, respectively, and for the dimensional characteristics base height (10), height to wrench (100), groove diameter (130) and groove depth (140) of the object PKR are shown, respectively, in Figure 5a–d. Each point in Figures 4 and 5 comes from a 25-measurement dataset.

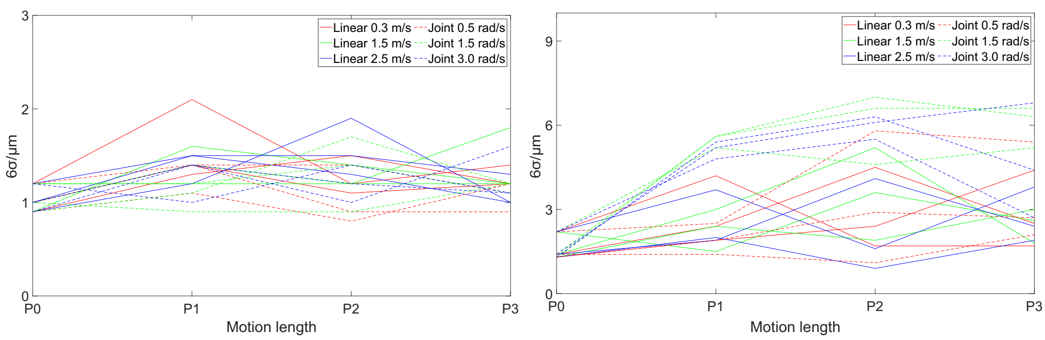

(**a**) Magnet diameter (Characteristic code 20) (**b**) Magnet height (Characteristic code 30)

Figure 4. Dimensional measurement variability (6σ) depending on the motion type (linear or joint motion), velocity, and the length of the motion for the dimensional characteristics magnet diameter (20) and magnet height (30) of the object magnet.

The points are linked with lines. The solid lines represent the measurements of linear motions and the dashed lines represent the measurements of joint motions. The solid red line represents the linear motion at a velocity of 0.3 m/s, the solid green line represents the linear motion at a velocity of 1.5 m/s, and the solid blue line represents the linear motion at a velocity of 2.5 m/s. The dashed red line represents the motion at joint velocities of 0.5 m/s, the dashed green line represents the motion at joint velocities of 1.5 m/s, and the dashed blue line represents the motion at joint velocities of 3.0 m/s. The movement's initial/ending poses P0, P1, P2, and P3 for a particular dataset appear on the horizontal line, while the 6σ values are on the vertical axes.

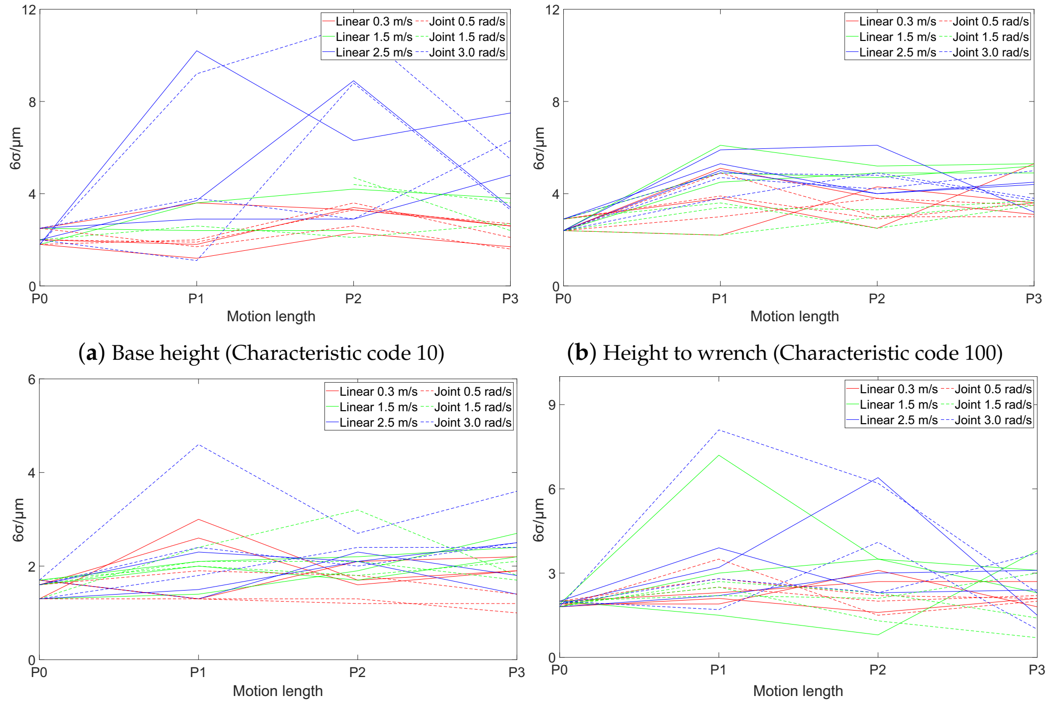

(**a**) Base height (Characteristic code 10) (**b**) Height to wrench (Characteristic code 100)

(**c**) Groove diameter (Characteristic code 130) (**d**) Groove depth (Characteristic code 140)

Figure 5. Dimensional measurement variability (6σ) depending on the motion type (linear or joint motion), velocity, and the length of the motion for the dimensional characteristics base height (10), height to wrench (100), groove diameter (130) and groove depth (140) of the object PKR.

4.2. Number of Active Joints

Figures 6 and 7 show the results of the study on the influence of the number of active joints on the measurements' variability. The calculated data of the geometric characteristics magnet diameter (20) and magnet height (30) of the object magnet are shown respectively in Figure 6a,b, while the measurements of the second part for all four geometric characteristics of the object PKR are shown respectively in Figure 7a–d for base height (10), height to wrench (100), groove diameter (130) and groove depth (140). The red colour presents a scenario with one active joint (W2—see Table 1), the green colour presents a scenario with two active joints (SE), the blue colour presents a scenario with three active joints (SEW1), and the black colour presents a scenario with four active joints (SEW1W2). In Figures 6 and 7, the solid lines present robot motions at joint velocities of 0.5 rad/s and the dashed lines present robot motions at joint velocities of 3.0 rad/s. The magnitudes of the joint's rotation ($\Delta\varphi = (0^\circ, 30^\circ, 60^\circ, 90^\circ)$ in the case of the scenario W2 and $\Delta\varphi = (0^\circ, 20^\circ, 40^\circ, 60^\circ)$ in the remaining cases) appear on the horizontal line.

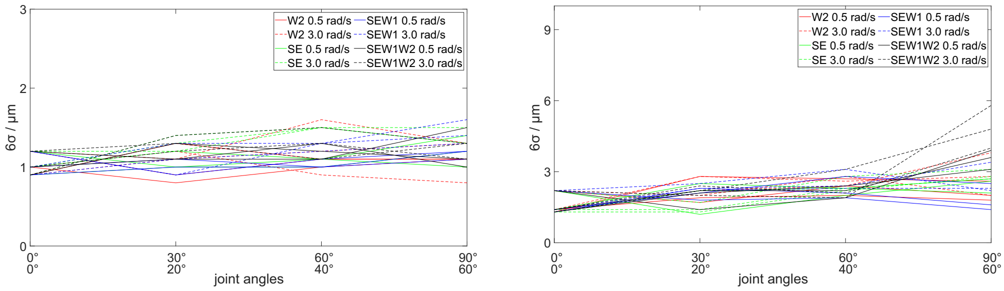

(**a**) Magnet diameter (Characteristic code 20) (**b**) Magnet height (Characteristic code 30)

Figure 6. Dimensional measurement variability (6σ) depending on the number of active joints, velocity, and the the joint's angle of motion for the dimensional characteristics magnet diameter (20) and magnet height (30) of the object magnet. Scenario W2 represents a robot's motion with one active robot joint, scenario SE represents the motion with two active joints, scenario SEW1 represents the motion with three active joints and scenario SEW1W2 represents the motion with four active joints.

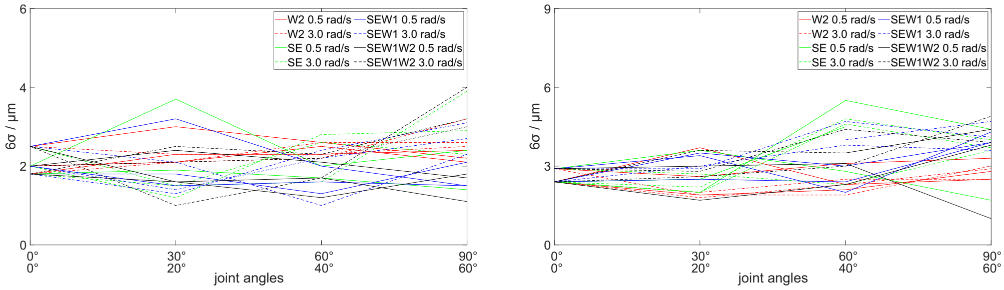

(**a**) Base height (Characteristic code 10) (**b**) Height to wrench (Characteristic code 100)

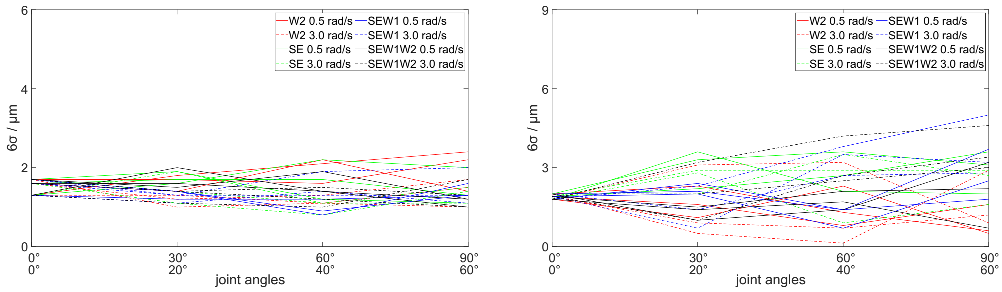

(**c**) Groove diameter (Characteristic code 130) (**d**) Groove depth (Characteristic code 140)

Figure 7. Dimensional measurement variability (6σ) depending on the number of active joints, velocity, and the joint angle of the motion for dimensional characteristics base height (10), height to wrench (100), groove diameter (130) and groove depth (140) of the object PKR. Scenario W2 represents the robot's motion with one active robot joint, scenario SE represents the motion with two active joints, scenario SEW1 represents the motion with three active joints and scenario SEW1W2 represents the motion with four active joints.

4.3. ANOVA

Figures 4–7 contain a lot of data represented by several lines, which in most cases overlap. To test whether individual measurement sets, representing one set of parameters (e.g., velocity, distance), are statistically significantly different from the other sets, the ANOVA method was used. Tables 2 and 3 summarise the results (F-values and p-values) of the ANOVA. The F-values and their corresponding p-values of the measurement variability for the motion type (linear or joint motion), the velocity of the motion, the length of the motion and their mutual interactions in the first scenario group of the measurements are gathered in Table 2.

Table 2. Calculated *F* and *p* values of the ANOVA statistical significance test in the first part of the measurements. The sources of the measurement variability are the robot's motion type (linear or joint motion), the velocity of the robot's motion, and the robot's motion length. Their mutual interactions (marked with ×) are also observed. The corresponding *F* and *p* values, which indicate the statistical significance of the sources for a given geometric characteristic of the objects, are written in bold.

Source (df)	*F*-Value (*p*-Value)					
	Magnet		PKR			
	20	30	10	100	130	140
Motion (1)	**5.97 (0.018)**	**28.38 (<0.001)**	0.03 (0.866)	**13.86 (<0.001)**	0.17 (0.679)	0.32 (0.577)
Velocity (2)	0.13 (0.876)	**5.51 (0.007)**	**15.53 (<0.001)**	**6.38 (0.003)**	**4.97 (0.010)**	2.69 (0.077)
Length (3)	**6.11 (0.001)**	**14.72 (<0.001)**	**5.71 (0.002)**	**23.58 (<0.001)**	**4.49 (0.007)**	**3.59 (0.019)**
Motion × Velocity (2)	0.30 (0.746)	**7.08 (0.002)**	0.07 (0.934)	**6.29 (0.003)**	**6.76 (0.002)**	1.64 (0.203)
Motion × Length (3)	1.07 (0.370)	**3.36 (0.025)**	0.43 (0.734)	1.65 (0.190)	0.48 (0.695)	0.27 (0.847)
Velocity × Length (6)	1.11 (0.367)	0.83 (0.553)	1.57 (0.175)	1.58 (0.170)	0.83 (0.555)	1.07 (0.391)

Table 3. Calculated *F* and *p* values of the ANOVA statistical significance test of the main effects and the mutual interactions (marked with ×) in the first part of the measurements. The sources of the measurement variability are the robot's motion type (linear or joint motion), the velocity of the robot's motion, and the robot's motion length. The corresponding *F* and *p* values, which indicate the statistical significance of the sources for a given geometric characteristic of the objects, are written in bold.

Source (df)	*F*-Value (*p*-Value)					
	Magnet		PKR			
	20	30	10	100	130	140
Scenario (3)	2.41 (0.074)	**4.79 (0.004)**	2.34 (0.081)	**5.17 (0.003)**	1.61 (0.195)	**6.49 (0.001)**
Velocity (1)	**16.94 (<0.001)**	**9.08 (0.004)**	**4.42 (0.039)**	1.45 (0.232)	**9.67 (0.003)**	**4.40 (0.039)**
Rotation (3)	**8.24 (<0.001)**	**32.35 (<0.001)**	**3.30 (0.025)**	**9.90 (<0.001)**	0.98 (0.410)	2.67 (0.054)
Scenario × Velocity (3)	1.11 (0.350)	0.92 (0.435)	1.53 (0.214)	2.00 (0.122)	**4.49 (0.006)**	**3.05 (0.034)**
Scenario × Rotation (9)	0.91 (0.520)	**6.43 (<0.001)**	0.52 (0.855)	1.76 (0.091)	1.18 (0.320)	1.97 (0.055)
Velocity × Rotation (3)	2.45 (0.071)	**3.89 (0.012)**	**12.22 (<0.001)**	1.24 (0.301)	1.67 (0.180)	2.18 (0.098)

Furthermore, the statistical *F*-values and *p*-values of the second group of measurements, where the interest was in the statistical significance of the measurement variability due to the number of active joints, the joint velocities and the magnitude of the joint rotation, are gathered in Table 3.

In both cases, the statistical parameters *F* and *p* are calculated for the magnet diameter (20) and magnet height (30) of the object magnet and the base height (10), height to wrench (100), groove diameter (130) and groove depth (140) of the object PKR. As usual, statistical significance can be considered if there is a *p*-value lower than $p_{min} = 0.05$.

The ANOVA results (*p*-values and *F*-values) indicate only statistical significance. Tables 4–9 present the mean variability (6σ) of the dimensional measurements for the analysis of the selected trajectory parameters. A comparison of variability between linear and joint motion is presented in Table 4, and a comparison of the number of active joints is presented in Table 7. Analysed data showing the influence of the motion velocity are presented in Tables 5 and 8, and are shown separately for the first and second parts. Statistical comparison data of motion length is presented in Tables 6 and 9. The rows in the tables represent the measured objects' dimensional characteristics, while the data in the columns represent the mean values of measurement variability (6σ) for the desired trajectory parameter.

Table 4. Calculated mean values of 6σ (in µm) for linear and joint motion statistical comparison.

Dimension	Linear	Joint
magnet 20	1.33	1.17
magnet 30	2.60	4.35
pkr 10	3.69	3.66
pkr 100	4.32	3.60
pkr 130	1.96	2.02
pkr 140	2.76	2.56

Table 5. Calculated mean values of 6σ (in µm) in the statistical comparison of velocity for the first part.

Dimension	Low	Medium	High
magnet 20	1.26	1.27	1.30
magnet 30	2.86	4.32	3.86
pkr 10	2.44	3.28	5.71
pkr 100	3.63	4.14	4.57
pkr 130	1.71	2.10	2.32
pkr 140	2.28	2.61	3.34

Table 6. Calculated mean values of 6σ (in µm) in motion length statistical comparison for the first part.

Dimension	P0	P1	P2	P3
magnet 20	1.03	1.34	1.28	1.21
magnet 30	1.63	3.37	3.99	3.68
pkr 10	2.10	3.45	4.51	3.54
pkr 100	2.57	4.29	3.99	4.05
pkr 130	1.53	2.07	2.01	2.04
pkr 140	1.90	3.12	2.83	2.29

Table 7. Calculated mean values of 6σ (in µm) in the statistical comparison of the number of active joints used to perform the robot motion.

Dimension	W2	SE	SEW1	SEW1W2
magnet 20	1.11	1.25	1.17	1.23
magnet 30	2.41	2.23	2.29	2.84
pkr 10	2.41	2.21	1.94	2.07
pkr 100	2.51	3.35	3.51	3.21
pkr 130	1.56	1.45	1.32	1.38
pkr 140	1.42	2.69	2.41	2.32

Table 8. Calculated mean values of 6σ (in µm) in the statistical comparison of velocity for the second part.

Dimension	Low	High
magnet 20	1.11	1.28
magnet 30	2.25	2.63
pkr 10	2.01	2.30
pkr 100	3.03	3.24
pkr 130	1.55	1.30
pkr 140	1.99	2.44

https://doi.org/10.3390/technologies14050261

Table 9. Calculated mean values of 6σ (in µm) in the statistical comparison of motion length for the second part.

Dimension	k = 0	k = 1	k = 2	k = 3
magnet 20	1.03	1.13	1.21	1.23
magnet 30	1.63	2.05	2.38	2.90
pkr 10	2.10	2.01	2.00	2.41
pkr 100	2.57	2.65	3.27	3.50
pkr 130	1.53	1.45	1.39	1.44
pkr 140	1.90	1.97	2.18	2.49

5. Discussion

This section covers two sets of experiments evaluating the effects of individual robot-trajectory parameters on the dimensional measurements presented in the Results Section. The comparison of linear and joint motion, motion velocity, and the length of motion in terms of dimensional measurement variability is emphasised as the first topic. Furthermore, the influence of the number of active joints required to perform the robot's motion, joint velocity, and the magnitude of joint rotation are other essential topics.

In a previous study, the impact of robot manipulation complexity on product dimensional measurement variability was identified. At that time, the broad concept was considered, but this time only one part of robot manipulation was focused on: the impact of robot motion–trajectory. We predicted that different trajectories, i.e., velocity, length or motion type, would affect the accuracy and repeatability of the robot's end-effector. Consequently, the position of the inserted object varies slightly, resulting in different touch locations with the touch probe in contact dimensional measurements and, thus, yielding different measured values.

As can be seen from a quick, simple observation of Figures 4–7, different robot trajectories have different effects on the measurements' variability. As expected, the differences in dataset variability across the individual scenarios are not as noticeable as in the previous study [45], where diverse contributions from grasping, re-grasping, and robot manipulation were sought. A general observation of Figures 4–7 shows that the absolute values of the measurements' variability obtained in the research coincide with those in scenario 7 presented in recent research. Furthermore, scenario 7 (total re-positioning) in the previous study corresponds to the scenario in the current research in the first part of the measurements, with the trajectory starting in pose P0, or at $\Delta\varphi = 0°$ in the second part.

5.1. Linear vs. Joint Movements

In the first part of the current measurements, the primary task was to investigate the possible influence of the motion type on the measurement variability. In other words, the question is whether the robot controller's algorithms, together with the resulting movement sets, affect the accuracy and repeatability of the robot's movement when carrying the measurement object.

A general observation could be obtained from the graphs in Figures 4 and 5, which present the analysed measurement data for linear and joint motion type (solid and dashed lines), three different velocities (different colours), and four different motion lengths (on the horizontal axis).

Please compare the curves for linear (solid lines) and joint motion (dashed lines) in the graphs in Figures 4 and 5. Initial observations indicate that the motion type affects the variability of the measurement dataset. The entire group of solid lines, which represent the linear motions of the robot end-effector, is slightly higher on the graphs than the group of dashed lines, which represent the robot's joint motions. This could be expressed more precisely as the robot's end-effector linear motions being reflected in greater variability across all the presented distances of the robot's motion.

Because there are many lines (for each repetition of the measurement set) in Figures 4 and 5, and many of them overlap, it is hard to interpret them with a high degree of certainty. Differences are present, but they are not as pronounced, as they can be distinguished from one another at a glance.

The data in Table 4 show higher mean dimensional measurement variability (6σ values) during object manipulation using robot linear motion. However, this is not true for the magnet diameter (30), since the table shows measurement variability that is much higher with joint motion 4.35 μm than with linear motion (2.60 μm). Higher variability using joint motion can also be observed in Figure 4b, where the majority of the dashed lines lie above solid lines, and the mean variability is almost twice as high as that of linear motion. Further, the differences in PKR characteristics 10 and 100 are not that significant.

According to the ANOVA statistical comparison shown in Table 2, the corresponding p-values for the motion type are lower than $p_{min} = 0.05$ for the magnet diameter (20) and magnet height (30) of the magnet object and the height to wrench (100) of the PKR object. The null hypothesis for those characteristics is rejected, resulting in two independent datasets (linear and joint motion). For the mentioned dimensional characteristics, the data in Table 4 show greater differences in the mean variability comparison. Thus, using linear and joint motion provides different and independent sets of measurements, and, combined with the data gathered in Table 4, influences the results of the advanced robot cell's dimensional measurements.

The difference in dataset variability between linear and joint motion is not large, but it is noticeable (Table 4, and Figure 4a,b). The practical difference between the motion types is that not all the robot joints need to be active in joint motion. Furthermore, the magnitude of the joint's rotations is smaller in the case of the joint motion. Also, joint rotation occurs in only one direction during a single motion. In the case of end-effector linear motion, the rotations of the active joints can be performed in both directions in order to follow the linear end-effector path. Consequently, more extensive joint angle rotations and rotation in both directions result in slightly larger positional and orientation errors of the robot end-effector, which explains the higher observed measurement variability.

When comparing Figures 4 and 5, it can also be argued that velocity potentially affects the measurement variability. The higher the velocity is, the greater the variability. On the graphs in Figures 4 and 5, the influence of velocity on the variability is understood based on a comparison of the red, green and blue lines. Red lines are generally lower than the green and blue lines for all four motion lengths and both motion types. In the case of the dimensional characteristics of the PKR object (Figure 5), it is also considered that the blue lines are placed higher than the red and green lines. In other words, the lowest velocities of the robot's motion contribute less variability to the measurements, while the highest velocities contribute the most. The differences in the values at different velocities are slight, but still perceptible.

An overall analysis of the data in Table 5 from left to right (from low to high robot motion velocity) generally indicates an increase in variability of dimensional measurements as the robot's velocity increases, which was previously observed in Figures 4 and 5. For magnet diameter (20), the increase in variability with increasing velocity is less pronounced than for the remaining dimensional characteristics.

The ANOVA statistical comparison presented in Table 2 confirms the alternative hypothesis H_1 for the characteristic magnet height (30) of the magnet object and the base height (10), height to wrench (100) and groove diameter (130) of the PKR object. The p-value of the characteristic groove depth (140) of the PKR object is approximately equal to the

https://doi.org/10.3390/technologies14050261

threshold value, and variability clearly increases with increased robot velocity (Table 5). Consequently, this characteristic could also be characterised by at least two statistically independent measurement sets.

Therefore, velocity can be considered an influencing factor in measurement variability, with increases up to 134% (pkr 10), though they are typically around 25–35%.

By considering Figures 4 and 5, it could be stated that the length of the robot's motion affects the Equator dataset variability. Indeed, the 6σ value is the lowest in the case of the minimum length of the motion (P0). The value of the measurement variability also increases slightly with the increasing length of the robotic motion or remains approximately the same. However, this trend is not pronounced.

Table 6 opposes the statement that dimensional measurement variability increases with the motion length. As shown in Figures 4 and 5, the mean variability is also the lowest for motions starting at point P0. Measurement variability increases with motion length, but it remains constant for P1, P2, and P3.

In contrast to the data in Table 6 and visual observations of the effect of the length of the motion in Figures 4 and 5, the results of the ANOVA calculations in Table 2 reject the null hypothesis for all six characteristics. ANOVA confirms the presence of independent data groups for different robot motion lengths (different mean values and similar variances), but this does not prove that there is an increase in variability with increasing motion length. Data analysis using ANOVA alone could be considered an influential parameter in the robot's trajectory, but calculated mean values should be considered as well.

The data in the first three lines of the Table 2 show that the change in the value of one influential parameter, for example, the length of the motion, results in at least two independent measurement groups with different measurement means; consequently, the statistical significance of the measurement groups can be stated. The mutual interactions among the influential parameters (marked with $\times$ in Table 2) are not statistically significant, as the null hypothesis is rejected in only 4 of 18 combinations of influential factors and geometrical characteristics. In other words, measurement groups have the same mean values.

5.2. Number of Active Joints

The results of the second part of the research are shown in Figures 6 and 7 for the object magnet and the object PKR, respectively, as well as in Tables 3, 7–9. The second part of the research focused on investigating the influence of the number of active joints on the dimensional measurement variability.

Figures 6 and 7 show the influence of the number of active joints in the robot's movement on the variability of the Equator measurements. The first observation of the curves in the figures mentioned above is that the number of active joints affects the 6σ values. The robot-motion scenario W2, where only one joint is active, generally results in a smaller dataset variability. The red lines, representing scenario W2, are placed lower than the other coloured lines in Figures 6a and 7b,d. In Figure 6b, all curves (all scenarios) are very condensed for the magnitude of the joint rotations at $\Delta\varphi = 0^\circ, 30^\circ, 60^\circ$(scenario W2) and $\Delta\varphi = 0^\circ, 20^\circ, 40^\circ$(scenarios SE, SEW1, SEW1W2). In the case of rotation at $\Delta\varphi = 90^\circ$ (scenario W2) and $\Delta\varphi = 60^\circ$ (scenarios SE, SEW1, SEW1W2), it can be argued again that measurements after the robot motions with scenario W2 have, on average, lower variability than the others.

For the characteristic groove diameter (130) of the PKR object (Figure 7c), by observing and comparing different coloured lines, it cannot be determined which scenario yields the lowest 6σ values. The measurement groups are very similar for all the robot-motion scenarios.

Considering the data in Table 7, the mean variability did not change significantly with an increase in the number of active joints used to perform robot motion, which was one of the main assumptions.

The ANOVA calculations in Table 3 show that the null hypothesis is rejected for the measurement sets of the characteristic magnet height (30) of the magnet object and the height to wrench (100) and groove depth (140) of the PKR object in scenarios with a different number of active joints, and border p-values for magnet diameter (20) of the magnet object and base height (10) of the PKR object. However, this analysis only tests the significant diversity among datasets. According to ANOVA calculations, the number of active joints could affect the variability of dimensional measurements, but the data in Table 7 contradict this.

In the previous part, it was shown that there is a difference in variability among different interpolation methods (linear and joint motion). However, here, the variability does not change with the increase in the number of active joints. As stated before, in linear end-effector motion, joint rotations can be performed in both directions and with different magnitudes of joint rotations. Comparing the mean values for the joint motion in Table 4 with data in Table 7 indicates lower mean variability for motion scenarios in the second part (investigating the number of active joints). In the latter case, all active joints rotated in the same direction, whereas in joint motion, this is not the case. Joint motion was performed with minimal rotation in each robot joint, and those rotations were not identical (as in the second part of the measurements).

As for the measurements in the first part, the velocity of the robotic motion also affects the second part of the measurements. In Figures 6 and 7, the dashed lines representing movements with higher joint velocities (3.0 rad/s) are, for the most part, above the solid lines representing movements at lower joint velocities (0.5 rad/s). At $\Delta\varphi = 30^\circ$ (W2) and $\Delta\varphi = 20^\circ$ (SE, SEW1 and SEW1W2) in Figure 7a,c, the solid lines are placed higher than the dashed ones. In all other cases, the dashed lines are above the solid ones, indicating higher measurement variability at higher joint velocities.

The influence of the robot motion in the second part is gathered in Table 8. Variability increases with increasing robot motion velocity. The change is not significant, but can be observed with an increase in variability that is typically up to 15%. In the groove diameter (characteristic 130) of the PKR object, the variability is higher at low robot velocity.

The second part of ANOVA rejects the null hypothesis for five geometrical characteristics: the magnet diameter (20) and magnet height (30) of the magnet object and the base height (10), groove diameter (130) and groove depth (140) of the PKR object (Table 3).

As mentioned in the first part of this paper, the robot's motion velocity can be considered an influential parameter in the variability of the dimensional measurements obtained with Equator after the robot's object manipulation. The variability increases with robot velocity.

The magnitude of joint rotations in the robot-manipulation scenarios in the second part of the measurements can also be understood as certain lengths of the robot's motions.

By considering Figures 6 and 7, a slight dependence of the measurement variability on the magnitude of the joint's rotation can be observed, with increasing variability across all curves from zero joint rotation to maximum joint rotation. This trend is more easily observed in Table 9, where increased joint rotation (higher k) leads to greater variability. Due to an increase in the joint rotation magnitude, variability increases by up to 78% (magnet 30), but typically increases by 20–30%. Variability results for the maximum joint rotation are similar to those for the motion length in the first part (Table 6). However, in this case, the increase in variability is gradual.

The ANOVA comparison of the measuring sets depending on the magnitude of the joint's rotation in Table 3 is very similar to the results of the statistical comparison of the measuring sets with different lengths of robot motions in the first part of the measurements (Table 2). In the case of various joint rotations, the null hypothesis H_0 is rejected for four dimensional characteristics (Table 3): the magnet diameter (20) and magnet height (30) of the magnet object and the characteristics base height (10) and height to wrench (100) of the PKR object.

5.3. Practical Implications

The results of the first part show that the motion type affects measurement variability, which is due to a slight end-effector pose displacement that occurs after inserting the object. The most significant trajectory parameter in this part is the motion velocity, with a typical increase of 20–25% in measurement variability. The motion length is not recognised as an influential parameter, since the variability increases at first but remains constant with further increases in motion length.

In the second part of the measurements, it could be noted that the different number of active joints does not yield statistically significant variability. An increase in variability is noted with the velocity increase, similar to that in the first part of the measurements. Lastly, the motion length has a visible impact on variability in the second part. The main difference in the second part of the measurements is that the joint rotations were all performed in the same nominal direction, whereas in the motion scenarios of the first part, they were not.

The obtained results can be incorporated into trajectory generation and optimisation, not only in measurement-based applications but also in precise pick-and-place operations.

Additionally, data can be obtained during the design and positioning of the measurement device in a fully robotised measurement environment, as well as during the pallet pose optimisation for measurement objects. Based on previous research, a minimum number of robot manipulation operations is suggested. Previous guidelines can be upgraded to use joint motion rather than linear motion, or to move with the minimum number of active joints at low to medium robot velocity. The last recommendation is to perform motions with minimum joint rotation as well.

In a robotised measurement application that is similar to the one presented, it is advisable to keep the measurement device and the pallet with the object close enough to achieve the minimum measurement variability using an optimal robot trajectory.

6. Conclusions

In product quality, there is an increasing emphasis on introducing automation and robotisation. However, despite popular belief, manipulation with a robot is not considered constant in many respects. Although the robot eliminates the operator's influence, it introduces new uncertainty into the measurement system.

In this study, the robot was used to serve the measuring device, allowing it to perform dimensional measurements. A slight displacement of the inserted object affects the variability of the contact dimensional measurements. The object's displacement results from a robot's manipulation; in this case, its trajectory. The motion type, velocity, motion length, and number of active joints were identified as potential influencing parameters on the robot's trajectory and, consequently, on the variability of the process measurement.

Analysed data, using measurement system analysis (MSA) and analysis of variance (ANOVA), clearly indicate that there is higher variability in the linear motion of the robot end-effector than in robot joint motion. Linear motion activates more robot joints to perform a desired motion than joint motion does between the same start and end poses. Each joint introduces a certain degree of positional uncertainty, and binding multiple active joints and segments into a kinematic chain further increases it.

However, among all the trajectory parameters considered, the number of active joints has the least amount of influence on dimensional measurement variability. The robot motion velocity has the highest impact on variability, followed by the length of the motion (or the magnitude of the joint rotation). With increased motion length and velocity, measurement variability also increases, especially in the second part of the measurements. The changes are not significant, but they are still noticeable.

Manipulation with a robot, even the motion trajectory, influences the object positioning. Different robot trajectories correspond to a minor (barely noticeable) displacement of the object inside the measuring device. This research is based on dimensional measurement acquisition with a single robot arm (UR5e) and it is limited to two workpieces. Future work will focus on the pose displacement detection to evaluate the displacement–variability correlation and tracking of the robot end-effector pose.

Author Contributions: Conceptualization, A.Z. and M.M.; methodology, A.Z.; software, A.Z.; validation, A.Z., and M.M.; formal analysis, A.Z.; investigation, A.Z.; resources, M.M.; data curation, A.Z.; writing—original draft preparation, A.Z.; writing—review and editing, A.Z. and M.M.; visualization, A.Z.; supervision, M.M.; project administration, M.M.; funding acquisition, M.M. All authors have read and agreed to the published version of the manuscript.

Funding: The authors acknowledge the financial support from the Slovenian Research Agency (research core founding No. P2-0228), and by the DIGITOP project under Grant No. TN-06-0106. The investment is co-financed by the Republic of Slovenia and the European Union under the Cohesion Fund/European Regional Development Fund/European Social Fund, project GOSTOP-Building Blocks, Tools and Systems for the Factories of the Future, Smart specialization, C3330-16-529000, 2016-20.

Institutional Review Board Statement: Not applicable.

Informed Consent Statement: Not applicable.

Data Availability Statement: The original contributions presented in this study are included in the article. Further inquiries can be directed to the corresponding author.

Acknowledgments: During the preparation this work authors used OpenAI models solely to improve language quality and readability. After using this tool/service, the authors reviewed and edited the content as needed and take full responsibility for the content of the submitted article.

Conflicts of Interest: The authors declare no conflicts of interest.

Abbreviations

The following abbreviations are used in this manuscript:

SPC	Statistical process control.
CMM	Coordinate measuring machine.
TCP	Tool centre point.
MSA	Measurement system analysis.
ANOVA	Analysis of variance.

References

1. Montgomery, D.C. *Introduction to Statistical Quality Control*, 4th ed.; John Wiley and Sons Inc.: Hoboken, NJ, USA, 2001.
2. Chandra, M.J. *Statistical Quality Control*; CRC Press: Boca Raton, FL, USA, 2001.

3. *Quality Management in the Bosch Group Technical Statistics. Booklet 10—Capability of Measurement and Test Processes*; Bosch: Stuttgart, Germany, 2010. Available online: https://assets.bosch.com/media/global/bosch_group/purchasing_and_logistics/information_for_business_partners/downloads/quality_docs/general_regulations/bosch_publications/booklet-no10-capability-of-measurement-and-test-processes_en.pdf (accessed on 22 April 2026).
4. Zhang, S.; Ajmal, A.; Wootton, J.; Chisholm, A. A feature-based inspection process planning system for co-ordinate measuring machine (CMM). *J. Mater. Process. Technol.* **2000**, *107*, 111–118. [CrossRef]
5. Takamasu, K.; Furutani, R.; Ozono, S. Basic concept of feature-based metrology. *Measurement* **1999**, *26*, 151–156. [CrossRef]
6. Weckenmann, A.; Eitzert, H.; Garmer, M.; Weber, H. Functionality-oriented evaluation and sampling strategy in coordinate metrology. *Precis. Eng.* **1995**, *17*, 244–252. [CrossRef]
7. Colosimo, B.M.; Moroni, G.; Petrò, S. A tolerance interval based criterion for optimizing discrete point sampling strategies. *Precis. Eng.* **2010**, *34*, 745–754. [CrossRef]
8. Lee, G.; Mou, J.; Shen, Y. Sampling strategy design for dimensional measurement of geometric features using coordinate measuring machine. *Int. J. Mach. Tools Manuf.* **1997**, *37*, 917–934. [CrossRef]
9. Bastas, A. Comparing the probing systems of coordinate measurement machine: Scanning probe versus touch-trigger probe. *Measurement* **2020**, *156*, 107604. [CrossRef]
10. Krawczyk, M.; Gaska, A.; Sladek, J. Determination of the uncertainty of the measurements performed by coordinate measuring machines. *tm-Tech. Mess.* **2015**, *82*, 329–338. [CrossRef]
11. Weckenmann, A.; Knauer, M.; Kunzmann, H. The Influence of Measurement Strategy on the Uncertainty of CMM-Measurements. *CIRP Ann.* **1998**, *47*, 451–454. [CrossRef]
12. Kritikos, M.; Concepción Maure, L.; Leyva Céspedes, A.A.; Delgado Sobrino, D.R.; Hrušecký, R. A Random Factorial Design of Experiments Study on the Influence of Key Factors and Their Interactions on the Measurement Uncertainty: A Case Study Using the ZEISS CenterMax. *Appl. Sci.* **2020**, *10*, 37. [CrossRef]
13. Kawalec, A.; Magdziak, M. Usability assessment of selected methods of optimization for some measurement task in coordinate measurement technique. *Measurement* **2012**, *45*, 2330–2338. [CrossRef]
14. Maresca, P.; Gómez, E.; Caja, J.; Barajas, C.; Berzal, M. Use of coordinate measuring machines and digital optical machines for the geometric characterization of circumference arcs using the minimum zone method. *Measurement* **2010**, *43*, 822–836. [CrossRef]
15. Forbes, A.B.; Mengot, A.; Jonas, K. Uncertainty associated with coordinate measurement in comparator mode. In *Laser Metrology and Machine Performance*; EUSPEN: Huddersfield, UK, 2015; pp. 146–155. Available online: https://www.euspen.eu/knowledge-base/LAMP15115.pdf (accessed on 22 April 2026).
16. Cheng, Y.; Wang, Z.; Chen, X.; Li, Y.; Li, H.; Li, H.; Wang, H. Evaluation and Optimization of Task-oriented Measurement Uncertainty for Coordinate Measuring Machines Based on Geometrical Product Specifications. *Appl. Sci.* **2019**, *9*, 6. [CrossRef]
17. Papananias, M.; Fletcher, S.; Longstaff, A.P.; Forbes, A.B. Uncertainty evaluation associated with versatile automated gauging influenced by process variations through design of experiments approach. *Precis. Eng.* **2017**, *49*, 440–455. [CrossRef]
18. Forbes, A.B.; Papananias, M.; Longstaff, A.P.; Fletcher, S.; Mengot, A.; Jonas, K. Developments in automated flexible gauging and the uncertainty associated with comparative coordinate measurement. In Proceedings of the *Euspen's 16th International Conference & Exhibition, Nottingham, UK, 30 May–3 June 2016*; European Society for Precision Engineering and Nanotechnology: Bedfordshire, UK, 2016; pp. 111–112.
19. Kiraci, E.; Palit, A.; Donnelly, M.; Attridge, A.; Williams, M.A. Comparison of in-line and off-line measurement systems using a calibrated industry representative artefact for automotive dimensional inspection. *Measurement* **2020**, *163*, 108027. [CrossRef]
20. Kiraci, E.; Franciosa, P.; Turley, G.A.; Olifent, A.; Attridge, A.; Williams, M.A. Moving towards in-line metrology: Evaluation of laser radar system or in-line dimensional inspection for automotive assembly systems. *Int. J. Adv. Manuf. Technol.* **2017**, *91*, 69–78. [CrossRef]
21. Altinisik, A.; Bolova, E. A comparison of off-line laser scanning measurement capability with coordinate measuring machines. *Measurement* **2021**, *168*, 108228. [CrossRef]
22. Lemes, S.; Strbac, D.; Cabaravdic, M. Using Industrial Robots to Manipulate the Measured Object in CMM. *Int. J. Adv. Robot. Syst.* **2013**, *10*, 281. [CrossRef]
23. Rosati, G.; Boschetti, G.; Biondi, A.; Rossi, A. On-line dimensional measurement of small components on the eyeglasses assembly line. *Opt. Lasers Eng.* **2009**, *47*, 320–328. [CrossRef]
24. Hashem, J.A.; Pryor, M.; Landsberger, S.; Hunter, J.; Janecky, D.R. Automating High-Precision X-Ray and Neutron Imaging Applications With Robotics. *IEEE Trans. Autom. Sci. Eng.* **2018**, *15*, 663–674. [CrossRef]
25. Czimmermann, T.; Chiurazzi, M.; Milazzo, M.; Roccella, S.; Barbieri, M.; Dario, P.; Oddo, C.M.; Ciuti, G. An Autonomous Robotic Platform for Manipulation and Inspection of Metallic Surfaces in Industry 4.0. *IEEE Trans. Autom. Sci. Eng.* **2022**, *19*, 1691–1706. [CrossRef]
26. Gabbar, H.A.; Idrees, M. ARSIP: Automated Robotic System for Industrial Painting. *Technologies* **2024**, *12*, 27. [CrossRef]

27. Saeidi Aminabadi, S.; Jafari-Tabrizi, A.; Gruber, D.P.; Berger-Weber, G.; Friesenbichler, W. An Automatic, Contactless, High-Precision, High-Speed Measurement System to Provide In-Line, As-Molded Three-Dimensional Measurements of a Curved-Shape Injection-Molded Part. *Technologies* **2022**, *10*, 95. [CrossRef]
28. Felix Offodile, O.; Ugwu, K. Evaluating the effect of speed and payload on robot repeatability. *Robot. Comput.-Integr. Manuf.* **1991**, *8*, 27–33. [CrossRef]
29. Offodile, O.F.; Ugwu, K.O.; Hayduk, L. Analysis of the Causal Structures Linking Process Variables to Robot Repeatability and Accuracy. *Technometrics* **1993**, *35*, 421–435. [CrossRef]
30. Brink, J.; Hinds, B.; Haney, A. Robotics repeatability and accuracy: Another approach. *Tex. J. Sci.* **2004**, *56*, 149–156.
31. Sirinterlikci, A.; Tiryakioğlu, M.; Bird, A.; Harris, A.; Kweder, K. Repeatability and Accuracy of an Industrial Robot: Laboratory Experience for a Design of Experiments Course. *Technol. Interface J.* **2009**, *9*, 1–10.
32. Mehrez, A.; Hu, M.; Offodile, O. Multivariate economic analysis of robot performance repeatability and accuracy. *J. Manuf. Syst.* **1996**, *15*, 215–225. [CrossRef]
33. Vocetka, M.; Huňady, R.; Hagara, M.; Bobovský, Z.; Kot, T.; Krys, V. Influence of the approach direction on the repeatability of an industrial robot. *Appl. Sci.* **2020**, *10*, 8714. [CrossRef]
34. Xu, B.; Yuan, L.; Yu, H. RBF Neural Network-Based Anti-Disturbance Trajectory Tracking Control for Wafer Transfer Robot Under Variable Payload Conditions. *Appl. Sci.* **2025**, *15*, 9193. [CrossRef]
35. Slamani, M.; Nubiola, A.; Bonev, I. Assessment of the positioning performance of an industrial robot. *Ind. Robot* **2012**, *39*, 57–68. [CrossRef]
36. Riemer, R.; Edan, Y. Evaluation of influence of target location on robot repeatability. *Robotica* **2000**, *18*, 443–449. [CrossRef]
37. Angelidis, A.; Vosniakos, G. Prediction and compensation of relative position error along industrial robot end-effector paths. *Int. J. Precis. Eng. Manuf.* **2014**, *15*, 63–73. [CrossRef]
38. Azadivar, F. The Effect of Joint Position Errors of Industrial Robots on Their Performance in Manufacturing Operations. *IEEE J. Robot. Autom.* **1987**, *3*, 109–114. [CrossRef]
39. Shiakolas, P.; Conrad, K.; Yih, T. On the Accuracy, Repeatability, and Degree of Influence of Kinematics Parameters for Industrial Robots. *Int. J. Model. Simul.* **2002**, *22*, 245–254. [CrossRef]
40. McGarry, L.; Butterfield, J.; Murphy, A. Assessment of ISO Standardisation to Identify an Industrial Robot's Base Frame. *Robot. Comput.-Integr. Manuf.* **2022**, *74*, 102275. [CrossRef]
41. Ferreras-Higuero, E.; Leal-Muñoz, E.; García de Jalón, J.; Chacón, E.; Vizán, A. Robot-process precision modelling for the improvement of productivity in flexible manufacturing cells. *Robot. Comput.-Integr. Manuf.* **2020**, *65*, 101966. [CrossRef]
42. Wu, L.; Ren, H. Finding the Kinematic Base Frame of a Robot by Hand-Eye Calibration Using 3D Position Data. *IEEE Trans. Autom. Sci. Eng.* **2017**, *14*, 314–324. [CrossRef]
43. Bock, M.; Perner, M.; Krombholz, C.; Beykirch, B. Relation between repeatability and speed of robot-based systems for composite aircraft production through multilateration sensor system. In *Proceedings of the Sensors and Smart Structures Technologies for Civil, Mechanical, and Aerospace Systems 2015*; International Society for Optics and Photonics, SPIE: Bellingham, WA, USA, 2015; Volume 9435, pp. 729–736. [CrossRef]
44. Makulavičius, M.; Petkevičius, S.; Bučinskas, V.; Dzedzickis, A. Quantitative Evaluation of an Industrial Robot Tool Trajectory Deviation Using a High-Speed Camera. *Machines* **2026**, *14*, 8. [CrossRef]
45. Zore, A.; Čerin, R.; Munih, M. Impact of a Robot Manipulation on the Dimensional Measurements in an SPC-Based Robot Cell. *Appl. Sci.* **2021**, *11*, 6397. [CrossRef]
46. Lemeš, S.; Čabaravdić, M.; Zaimović-Uzunović, N. Robotic manipulation in dimensional measurement. In *Proceedings of the 2013 XXIV International Conference on Information, Communication and Automation Technologies (ICAT)*; IEEE: Piscataway, NJ, USA, 2013; pp. 1–7. [CrossRef]
47. Sivaji, A. Measurements System Analysis. In *Proceedings of the Third IEEE International Workshop on Electronic Design, Test and Applications*; DELTA '06; IEEE Computer Society: Washington, DC, USA, 2006; pp. 393–396.
48. Anderson, T.W.; Darling, D.A. Asymptotic Theory of Certain "Goodness of Fit" Criteria Based on Stochastic Processes. *Ann. Math. Stat.* **1952**, *23*, 193–212. [CrossRef]
49. Brown, M.B.; Forsythe, A.B. Robust tests for the equality of variances. *J. Am. Stat. Assoc.* **1974**, *69*, 364–367. [CrossRef]

https://doi.org/10.3390/technologies14050261